Received: July 1, 2024. Revised: July 31, 2024.

International Journal of
Intelligent Engineering & Systems

http://www.inass.org/

Stability Improvement of Hybrid Renewable Energy Systems by Using Virtual Inertia Controller Based on Optimized FOPID with Harris Hawk Optimization

Imam Robandi[1]* Mohamad Almas Prakasa[1] Muhammad Ruswandi Djalal[1]
Akhmad Ramadhani[1] Vita Lystianingrum Budiharto Putri[1] Rony Seto Wibowo[1]

[1]*Department of Electrical Engineering, Institut Teknologi Sepuluh Nopember (ITS), Surabaya 60111, Indonesia*
* Corresponding author's Email: imam.robandi@its.ac.id

Abstract: Virtual Inertia (VI) emulation becomes crucial to improve the stability of Hybrid Renewable Energy Systems (HRES). VI emulation needs a proper VI Controller (VIC) to adapt in various working conditions. This paper proposes the stability improvement of HRES with VIC based on optimized Fractional Order Proportional-Integral-Derivative (FOPID) with Harris Hawk Optimization (HHO). The proposed method is implemented on HRES that consists of Photovoltaic Energy Systems (PVES), Wind Energy Systems (WES), Synchronous Generator Energy Systems (SGES), and Energy Storage Unit (ESU). Based on the statistical assessment and convergence curve analysis, HHO performance in finding the optimal parameters is 31.98% to 41.62% better than the other well-known algorithms. Besides that, the VIC-FOPID-HHO gives the best stability improvement compared to basic PID and the other algorithms. In uncertain behavior of RES scenarios, the improvement by VIC-FOPID-HHO is indicated by frequency nadir reduction up 89.44%, overshoot reduction up to 98.45%, and better settling time up to 61.48%. In multi-level load shedding scenarios, the improvement by VIC-FOPID-HHO is indicated by frequency nadir reduction up 93.67%, overshoot reduction of up to 97.4%, and better settling time of up to 49.94%.

Keywords: FOPID controller, Harris hawk optimization, Hybrid renewable energy system, Stability improvement, Virtual inertia controller.

1. Introduction

The modern power system trend is the topological shift of the power electricity system from centralized to decentralized [1]. Decentralized power systems utilize Renewable Energy Sources (RES) as the popular option due to their flexibility constructed based on their potential in specific sites. The RES utilization ranges from small-scale (ex: household, independent office, etc.) to large-scale power electricity systems (ex: industrial, community building, etc.) [2]. Besides that, RES utilization allows electricity consumers to build their systems. In addition, RES supports the power and energy systems with specific strategies, like frequency regulation, energy buffers, complement energy sources, etc.

Besides the advantages, RES utilization poses typical challenges due to the uncertain and intermittent energy sources based on natural conditions. Thus, the Hybrid Renewable Energy Systems (RES) is developed [3]. Combining two or more sources can increase the reliability of supplying power electricity. Moreover, the Energy Storage Unit (ESU) is also combined to ensure continuity. The other challenge in RES is the lack of reactive power supplies which makes this system need additional components like a Static VAR Compensator (SVC) [4]. Besides that, the in-depth investigation shows that the dynamic stability related to minor signal disturbances needs special attention due to the wider working conditions than conventional power systems [5].

The stability challenge in HRES is typically caused by the deficiency of damping and inertia properties [6]. In conventional power electricity systems consisting of traditional generators, the damping and inertia properties can be maintained by regulating the mechanical parts. On the other hand,

most of the HRES mainly consists of power electronics with the absence of damping and inertia properties. Thus, the majority of HRES is called an inertia-less system. In inertia-less systems, the oscillation caused by minor signal disturbances that bother the stability needs different treatments from conventional ones. The additional stability controller, like the Power System Stabilizer (PSS), is no longer effective in enhancing the stability of HRES [7, 8]. Thus, the Virtual Inertia (VI) concept is developed as a viable solution.

The VI imitates the inertia in conventional generators by regulating the behavior of the ESU and inverter via the Virtual Inertia Controller (VIC) [6]. VIC scheme is strongly related to the Rate of Change of Frequency (RoCoF). The typical RoCoF in HRES is higher than in conventional generator systems causing the frequency nadir. In the VIC, the RoCoF is used as a signal reference to calculate the additional amount of inertia needed to improve the frequency nadir. Thus, the ESU and inverter can be regulated by VIC to inject the additional electricity power at a specific time [9]. The additional electricity power in exact time has a similar effect with the opposite torque provided by the mechanical part in the conventional generator. Thus, VIC optimization is crucial in the stability improvement of HRES.

Most of the existing literature dispatches the basic VIC consisting of virtual damping (D_{VI}) and virtual inertia (K_{VI}) that need to be tuned [7, 8, 10, 11]. Currently, VIC is popular to be combined with well-known controllers: Fuzzy Logic Controller (FLC) or Proportional-Integral-Derivative (PID) controller [12, 13]. Moreover, the Fractional Order PID (FOPID) has been developed and offered a better controller effect than the basic ones. [14, 15]. This trend effectively increases the stability improvement effect, however making the parameter tuning more complex. In the intelligent algorithm era, learning-based and metaheuristic algorithms become viable options for tuning the parameters [16, 17]. In addition, the metaheuristic is more popular than learning-based algorithms due to its easiness of implementation. It also has a superior ability to track the optimal solutions.

Various recent algorithms have been implemented for controlling the parameters of PID or FOPID. Recent algorithms have been developed with complex operations and outstanding inspiration in the world, such as the Flower Pollination Algorithm (FPA) [18], Manta Ray Foraging Algorithm (MRFA) [12], Firefly Algorithm (FA) [19], and Harris Hawk Optimization (HHO) [20, 21], etc [17]. HHO is one of the most popular algorithms since it was invented in 2019. HHO is inspired by the unique hunting mechanism of Harris Hawk to construct dynamic solution tracking in the exploration and exploitation processes [22-24]. HHO is proven as the settled algorithm due to its superiority in very wide research implementation. Moreover, HHO is widely used as a benchmark algorithm in newer algorithm comparisons. The results show that HHO still competes with the newer algorithms. Nowadays, recent algorithms with simple inspirations like Arithmetic Optimization Algorithm (AOA) and Equilibrium Optimization Algorithm (EOA) have also appeared [25–27]. HHO needs further comparisons and extended implementation in the VIC and FOPID cases due to its still limited in the current literature.

Most of the VIC investigations are focused on the inertia level of the systems [6]. Whereas the comprehensive investigation on wider working conditions, especially in uncertain behavior of RES and load shedding. With the motivation to provide a novel solution to the current trend within the mentioned challenges, this paper proposes a novel method to improve the stability of HRES with significant contributions stated in the following.

1) Proposing stability improvement in HRES by using the VIC based on optimized FOPID with HHO. The FOPID is compared with the basic PID controller. Besides that, HHO is compared with the AOA and EOA. The comparison is expected to extend the dominance of HHO over the newer well-known algorithms, especially in power system applications.

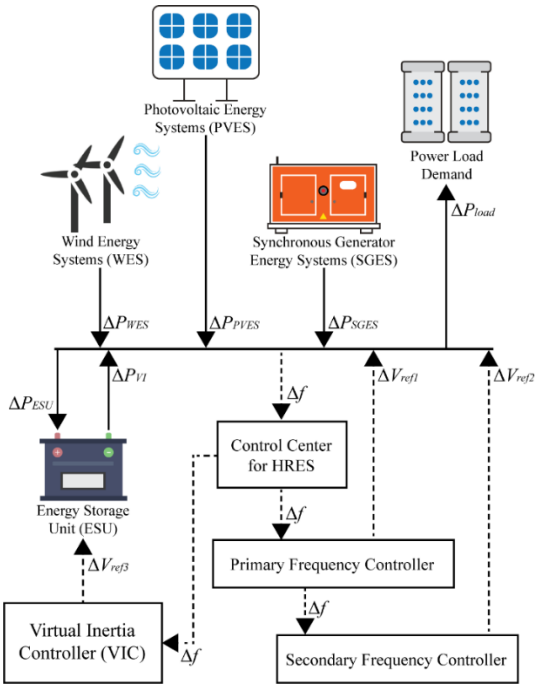

Figure. 1 Synoptic diagram for investigated HRES

2) Providing in-depth investigation for the performance of VIC-FOPID-HHO using statistical assessment and time domain simulation when several critical conditions occur. In this paper, two scenarios are considered as follows: 1) the fluctuation and uncertainties of RES in supplying power load demand; 2) multi-level sudden power load shedding.

This paper is organized as follows: The proposed test models for HRES and controller are constructed in Section 2. The proposed method, consisting of problem definition and algorithm, is described in Section 3. The performance of the VIC-FOPID-HHO is investigated in Section 4. In the rest, the main findings are justified in Section 5.

2. Design of the HRES and controller

In this section, HRES and controller structures are given in a synoptic diagram as in Fig. 1. HRES is designed with Synchronous Generator Energy Systems (SGES), and two RES generators: Wind Energy Systems (WES) and Photovoltaic Energy Systems (PVES). The Energy Storage Unit (ESU) is also dispatched to realize the VI emulation. All components are connected via a tie-line to supply the power load demand. The control center for HRES is established for RoCoF (Δf) monitoring as a stability reference. This design consists of three frequency-based stability controllers: primary controller, secondary controller, and VIC.

2.1 HRES design

The detailed block diagram of the system is given in Fig. 2. The models are designed in a simplified form to emphasize the focus investigation of the dynamic behavior of the system. The HRES model is modified from Ref. [6] and [28]. The relations between components in HRES are described by 5th-order mathematical equations as given in Eq. (1) until Eq. (5).

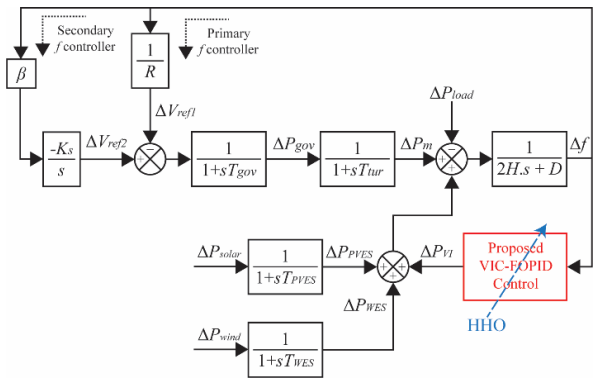

Figure. 2 Block diagram for HRES

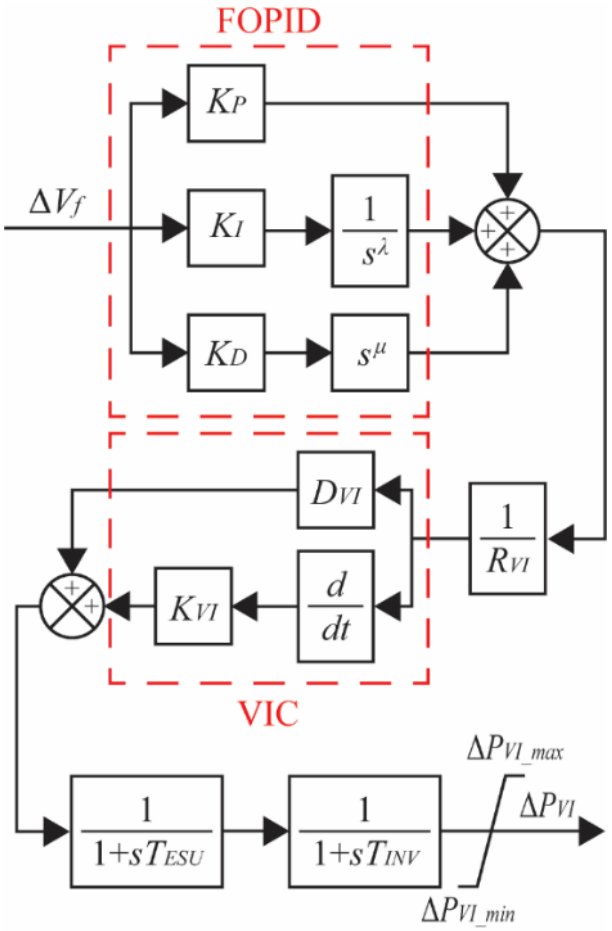

Figure. 3 Block diagram for proposed VIC-FOPID

$$\dot{\Delta f} = \frac{1}{2H}(\Delta P_m + \Delta P_{PVES} + \Delta P_{WES} + \Delta P_{load}) - \frac{D}{2H} \cdot \Delta f \quad (1)$$

$$\Delta \dot{P}_m = -\frac{1}{T_{tur}}(\Delta P_m) + \frac{1}{T_{tur}}(\Delta P_{gov}) \quad (2)$$

$$\Delta \dot{P}_{gov} = -\frac{1}{T_{gov}}(\Delta P_{gov}) - \frac{1}{R.T_{gov}} \cdot \Delta f + \frac{1}{T_{gov}}(\Delta V_{ref2}) \quad (3)$$

$$\Delta \dot{P}_{PVES} = \frac{1}{T_{PVES}}(\Delta P_{solar}) - \frac{1}{T_{PVES}}(\Delta P_{PVES}) \quad (4)$$

$$\Delta \dot{P}_{WES} = \frac{1}{T_{WES}}(\Delta P_{wind}) - \frac{1}{T_{PWES}}(\Delta P_{WES}) \quad (5)$$

with Δf is RoCoF. H and D are the inertia and damping properties, respectively. ΔP_m is change of mechanical power from SGES; ΔP_{PVES} is change of PVES output dependent on solar irradiation level (ΔP_{solar}) and time response of PVES (T_{PVES}); ΔP_{WES} is change of WES output dependent on wind speed level (ΔP_{wind}) and time response of WES (T_{WES}). The power sources are combined to supply

the power load demand (ΔP_{load}). T_{tur} and T_{gov} are the time responses of the turbine and governor in SGES, respectively. ΔP_{gov} is generated power in the turbine. ΔV_{ref1} is reference signal from the primary f controller with the speed droop controller ($1/R$). ΔV_{ref2} is reference signal from the secondary f controller with bias factor (β) and constant (K_s). ΔV_{ref3} is a reference signal for ESU to generate VI emulation (ΔP_{VI}).

In this paper, the state-space model for HRES is given by Eq. (6) and Eq. (7).

$$\dot{X} = AX + BU \tag{6}$$

$$Y = CX + DU \tag{7}$$

with X is the observed variable as given in Eq. (8), U is minor signal disturbances as given in Eq. (9), and Y is the observed output as given in Eq. (10). In this paper, minor signal disturbances are considered by ΔP_{solar}, ΔP_{wind}, and ΔP_{load}.

$$X = [\Delta P_m \quad \Delta P_{PVES} \quad \Delta P_{WES} \quad \Delta P_{VI} \quad \Delta f] \tag{8}$$

$$U = [\Delta P_{solar} \quad \Delta P_{wind} \quad \Delta P_{load}] \tag{9}$$

$$Y = [\Delta f] \tag{10}$$

2.2 Proposed VIC-FOPID design

The proposed controller is shown in Fig. 3. The VIC-FOPID uses Δf as input references for indicating the stability of the power system. Thus, the equation of FOPID is given by Eq. (11) [29].

$$\Delta V_{FOPID} = K_P \left(1 + \frac{K_I}{s^{\lambda}} + K_D s^{\mu}\right) \Delta f \tag{11}$$

with K_P, K_I, and $K_D$are the gains of the proportional, integral, and derivative components, respectively. Besides that, λ and μ are the fractional orders.

The output of the FOPID controller (V_{FOPID}) is fed to VIC. Thus, the equation for VIC as in Ref. [7], can be modified as given in Eq. (12).

$$\Delta P_{VI} = \left[\frac{sK_{VI}+D_{VI}}{(1+sT_{INV})(1+sT_{ESU})}\right] \cdot \left[\frac{\Delta V_{FOPID}}{R_{VI}}\right] \tag{12}$$

with P_{VI} is power emulated by VI. K_{VI} and D_{VI} are gains of virtual inertia and virtual damping, respectively. T_{INV} and T_{ESU} are time responses for inverter and ESU, respectively. R_{VI} is the constant of virtual inertia droop.

Table 1. Tuneable parameter

Parameter	Lower Bound (B_L)	Upper Bound (B_U)
K_P	0.01	2
K_I	0.01	2
K_D	0.01	2
λ	0.01	2
μ	0.01	2
K_{VI}	0.1	2
D_{VI}	0.1	20

3. Proposed optimization method

In this section, the optimization method for VIC-FOPID based on HHO is presented. First, the problem definition is described. Second, the implementation of HHO is explained.

3.1 Problem definition

This paper aims to improve the stability of the HRES. Stability can be obtained by investigating the eigenvalue of the system or the performance indexes from the observed response [30]. The second choice offers easiness and flexible utilization for special cases, like optimizing VIC-FOPID using HHO. Thus, the Integral Time Absolute Error (ITAE) is formulated as an objective function in Eq. (13).

$$\min(ITAE) = min\left[\int_0^{T_{sim\_max}} t|e(t)|\, dt\right] \tag{13}$$

with T_{sim_max} is the maximum of the time simulation.

The tuneable parameters and their typical search space are described in Table 1 [7, 19, 31]. Besides that, the eigenvalue and damping ratio calculation in Eq. (14) and Eq. (15) are needed to constrain the optimal solution tracking as in Eq. (16) and Eq. (17) [7, 8].

$$\lambda_{eig} = \sigma_{eig} + \omega_{eig} \tag{14}$$

$$\xi_{eig} = \frac{-\sigma_{eig}}{\sqrt{\sigma_{eig}^2+\omega_{eig}^2}} \tag{15}$$

$$\sigma_{eig\_1} \leq \sigma_{eig\_0} \tag{16}$$

$$\xi_{eig\_1} \geq \xi_{eig\_0} \tag{17}$$

with λ_{eig} is the eigenvalue of the system consisting of σ_{eig} and ω_{eig} that represents the damping and oscillation factors, respectively. ξ_{eig} is the damping ratio. σ_{eig_1} and σ_{eig_0} are the damping factors

before and after optimization, respectively. ξ_{eig_1} and ξ_{eig_0} are the oscillation factors before and after optimization, respectively.

3.2 HHO as optimizer

HHO is developed with the emulation of the animal intelligence of Harris Hawks in hunting their prey [21, 22]. These hawks have unique strategies to explore and exploit their prey in a cooperative group dynamically. HHO is described in four phases: pre-hunting, exploration, transition, and exploitation [7, 8].

3.2.1. Pre-hunting

In this phase, the hawks form a group with certain members (N_{pop}). The hawks spread in a certain direction to observe the potential prey. The initial position of the hawks (H_i) is given by Eq. (18). The bounds are determined from Table 1. The dimension (D) is defined based on the number of tuneable parameters.

$$H_i = (B_L \leq H_i \leq B_U)^D \quad (18)$$

The initial position of the prey considered as a rabbit (R_i) is also generated. R_i represents the potential best solution. The initial fitness value of R_i is calculated based on Eq. (13). It is defined as the initial energy of the rabbit (E_o) as in Eq. (19) to calculate the escaping energy of the rabbit (E_{esc}) along the iterations (T).

$$E_{esc} = 2E_o\left(1 - \frac{T}{T_{max}}\right) \quad (19)$$

3.2.2. Exploration

If the rabbit has been spotted, then the hawks observe and monitor the current condition of the rabbit. The movements of the hawks are defined based on q. If $q \geq 0.5$, then the hawks move randomly as in Eq. (20). While $q < 0.5$, then the hawks surround the rabbit as in Eq. (21).

$$H(T+1) = H_{rand}(T) - r_1|H_{rand}(T) - 2r_2H(T)| \quad (20)$$

$$H(T+1) = [R(T) - H_m(T)] - r_3[B_U + r_4(B_U - L_B)] \quad (21)$$

with $H(T)$ and $H(T+1)$ are the positions of the hawks in the current and the next iteration, respectively. H_{rand} is the random hawks. H_m is average of the position of the hawks. r_1, r_2, r_3, and r_4 are randomly uniform distribution values between 0 to 1.

3.2.3. Transition

The hawks monitor the condition of the rabbit in real time to decide when the hunting process will be started. $E_o = 0 \rightarrow 1$ means the rabbit has a lot of escaping energy. While $E_o = 1 \rightarrow 0$ means the rabbit has run out of escaping energy. Thus, if $|E_{esc}| \geq 1$, then the hawks are still in the exploration phase. While $|E_{esc}| < 1$, then the hawks are starting the exploitation phase.

3.2.4. Exploitation

The hawks have four different strategies to exploit the rabbit. The strategies are dynamically changed based on $|E_{esc}|$ and the probability of the rabbit escaping (r_{esc}). $r_{esc} \geq 0.5$ means the rabbit has a small chance of escaping. While $r_{esc} < 0.5$ means the rabbit has a big chance of escaping. In this phase, the rabbit makes a jumping movement as $J = 1 - r_5$, with r_5 is a random value between 0 to 1.

Soft besiege strategy is performed when $|E_{esc}| \geq 0.5$ and $r_{esc} \geq 0.5$. The hawks encircle and perform soft besieges to tire the rabbit. The movement of the hawks is updated based on Eq. (22).

$$H(T+1) = \Delta H(T) - E_{esc}|JR(T) - H(T)| \quad (22)$$

with $\Delta H(T)$ is the difference between the hawks and the rabbit.

Hard besiege strategy is performed when $|E_{esc}| < 0.5$ and $r_{esc} \geq 0.5$. The rabbit seems to get tired, thus the hawks perform heavy attacks to shock and catch the rabbit quickly. The movement of the hawks is updated based on Eq. (23).

$$H(T+1) = R(T) - E|\Delta H(T)| \quad (23)$$

Soft besiege with progressive rapid dives strategy is performed when $|E_{esc}| \geq 0.5$ and $r_{esc} < 0.5$. The rabbit has a lot of energy, thus it moves with Levy Flight (LF) movement as in [22]. If $F(R_Y) < F(H(T))$, then the hawks predict the next movement of the rabbit (R_Y) as in Eq. (24).

$$H(T+1) = R_Y = R(T) - E|JR(T) - H(T)| \quad (24)$$

If the hawks have failed to catch the rabbit $F(R_W) < F(H(T))$, then the hawks re-estimate the next movement of the rabbit (R_W) as in Eq. (25).

$$H(T+1) = R_W = R_Y + S \times LF(D) \quad (25)$$

Table 2. HRES parameters

Parameter	H	D	T_{tur}	T_{gov}	K_s	R
Value	7.2	0.8	0.56	0.32	0.35	14.6
Parameter	β	T_{PVES}	T_{WES}	T_{ESU}	T_{INV}	
Value	19.8	1.8	1.3	0.05	0.01	

Table 3. Simulation scenarios

No.	Disturbance (p.u.)	T_{sim} (s)			
		0	2	7	12
I	ΔP_{load}	0	+0.01	+0.02	+0.005
	ΔP_{solar}	0	+0.006	+0.004	+0.002
	ΔP_{wind}	0	+0.003	+0.014	+0.002
	ΔP_m	0	+0.001	+0.002	+0.001
II	ΔP_{load}	0	-0.005	-0.002	-0.001
	ΔP_{solar}	0	+0.001	-	-
	ΔP_{wind}	0	+0.002	-	-
	ΔP_m	0	-0.008	-0.002	-0.001

with S is a randomly generated matrix with $1 \times D$.

Hard besiege with progressive rapid dives strategy is performed when $|E_{esc}| < 0.5$ and $r_{esc} < 0.5$. the rabbit is getting exhausted due to continued besieging from the hawks. The hawks perform heavy attacks repeatedly until the rabbit is caught. The movements are updated based on the new R_Y as in Eq. (26). While the R_W is similar to Eq. (25).

$$H(T+1) = R_Y = R(T) - E|JR(T) - H_m(T)| \quad (26)$$

The hunting process will be finished when the hawks are successful in catching the rabbit. It indicated with $|E_{esc}| \rightarrow 0$.

4. Simulation and discussion

In this paper, the HRES is simulated in MATLAB/Simulink using parameters in Table 2. Besides that, the different simulation scenarios with the specific cases are arranged based on the the uncertain behavior of RES in supplying the power load demand and multi-level sudden power load shedding as detailed in Table 3.

Scenario I is arranged to investigate the effect of fluctuation and uncertainties of P_{WES} and P_{PVES} dependent on the ΔP_{wind} and ΔP_{solar}, respectively. Scenario I simulates three different conditions continuously as follows: 1) At $T_{sim} = 2$, the simulation investigates the condition if ΔP_{solar} is higher than P_{wind}; 2) At $T_{sim} = 7$, the simulation investigates the condition if ΔP_{solar} is lower than P_{wind}. The ΔP_{load} in Case 2 is bigger than Case 1 due to the assumption that WES has more stable electricity output than PVES; and 3) At $T_{sim} = 12$, the simulation investigates the condition if ΔP_{solar} is equal to P_{wind}.

Scenario II is arranged to investigate the effect of multi-level load shedding. Scenario II also contains three cases simulated continuously as follows: 1) At $T_{sim} = 2$, it simulates the condition that the sudden load shedding occurs when the RES is still supplying the load demand. Thus, the SGES should reduce ΔP_m significantly to avoid the excess power supplied; 2) At $T_{sim} = 7$, the RES is not supplying the load demand anymore. Thus, the ΔP_m is only adjusted depending on ΔP_{load}; and 3) At $T_{sim} = 12$, it simulates a similar condition with Case 2 in the lower ΔP_{load} value.

Table 4. Statistical comparison of optimal fitness value conducted by VIC-FOPID-HHO

No.	Stats.	Optimizer		
		AOA	EOA	HHO
VIC-FOPID				
1	*Avg.*	9.4 x 10^{-3}	1.18 x 10^{-2}	2.89 x 10^{-3}
	Std.dev.	6.75 x 10^{-3}	1.03 x 10^{-2}	7.48 x 10^{-4}
II	*Avg.*	1.71 x 10^{-2}	2.34 x 10^{-2}	8.63 x 10^{-3}
	Std.dev.	1.75 x 10^{-2}	2.14 x 10^{-2}	1.2 x 10^{-2}
VIC-PID				
1	*Avg.*	1.13 x 10^{-2}	1.24 x 10^{-2}	1.11 x 10^{-2}
	Std.dev.	1.25 x 10^{-3}	2.11 x 10^{-3}	1.68 x 10^{-3}
II	*Avg.*	4.08 x 10^{-2}	2.35 x 10^{-2}	2.32 x 10^{-2}
	Std.dev.	2.69 x 10^{-2}	6.37 x 10^{-4}	4 x 10^{-6}

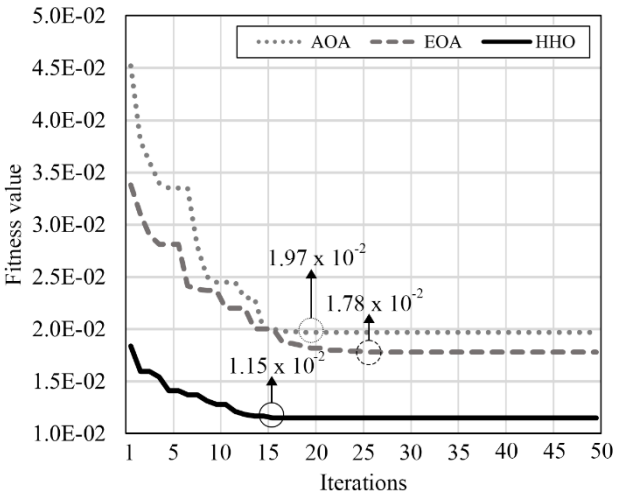

Figure. 4 Convergence curve comparison of average fitness value of the algorithms

4.1 Statistical assessment

The statistical comparison between the proposed methods and the other well-known algorithms is tabulated in Table 4. HHO is compared with EOA and AOA. The statistical results are collected within 100 iterations in 30 runs. The statistical results measure the performances of the algorithms.

Due to the objective function in Eq. (13) aims to minimize the ITAE, thus better accuracy and consistency can be indicated by lower average (*Avg.*) and lower standard deviation (*Std.dev.*) of the fitness values, respectively. From Table 4, the superiority of HHO over AOA and EOA in optimizing VIC-FOPID and VIC-PID is observable due to it producing the lowest *Avg.* and *Std.dev.* of fitness values in almost all cases. It means the HHO has the best accuracy and consistency over the compared algorithms in tackling optimization cases in this paper.

4.2 Convergence curve analysis

The process of the algorithms in finding the best solution is illustrated in the convergence curve as given in Fig. 4. This curve represents the performance of the algorithms in exploring and exploiting the best candidate solutions. Based on Fig. 4, HHO conducts the lowest value since the first iteration until the convergence result is achieved. The convergence curves of all algorithms are acceptable due to not being stuck in local optima. Besides that, HHO is the fastest algorithm to achieve its convergence within 16 iterations, which is followed by AOA and EOA within 19 and 26 iterations, respectively. Moreover, the average lowest fitness value conducted by HHO is 1.15 x 10^{-2}, which is 41.62% and 31.98% better than AOA of 1.97 x 10^{-2} and EOA of 1.78 x 10^{-2}, respectively.

Table 5. Optimal parameters for VIC-FOPID and VIC-PID by AOA, EOA, and HHO

Optimizer	VIC-FOPID Parameters							VIC-PID Parameters				
	K_P	K_I	K_D	λ	μ	K_{VI}	D_{VI}	K_P	K_I	K_D	K_{VI}	D_{VI}
Scenario I								**Scenario I**				
AOA	1.744	1.091	0.751	0.967	0.371	0.01	19.657	1.998	1.993	0.01	0.01	19.993
EOA	1.712	0.91	0.561	1.421	0.088	0.01	11.048	1.982	2	1.182	0.01	20
HHO	2	1.956	2	1.956	1.242	0.01	19.564	1.845	1.982	0.041	0.612	19.921
Scenario II								**Scenario II**				
AOA	1.355	1.401	0.01	1.993	0.01	1.038	13.149	1.903	0.04	0.01	0.01	18.982
EOA	1.83	1.782	0.01	0.601	1.503	0.01	9.115	1.903	2	0.312	0.01	19.941
HHO	1.753	1.998	0.01	0.011	0.01	0.04	20	1.113	1.989	1.559	0.01	20

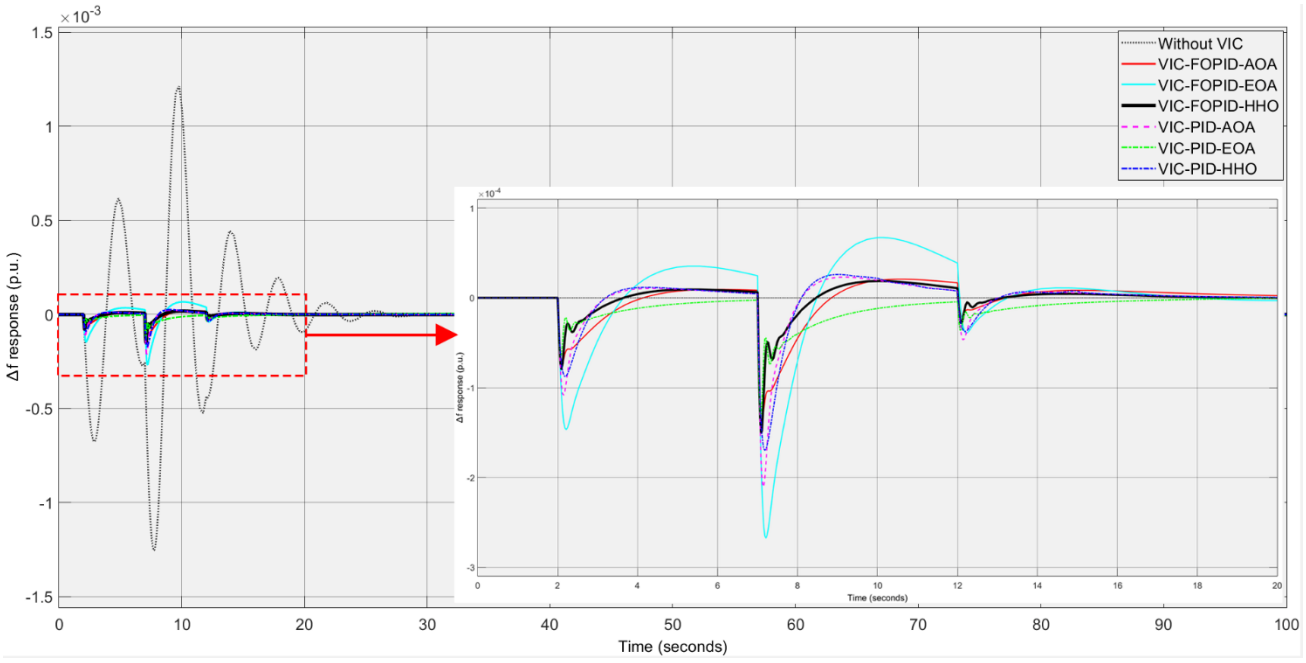

Figure. 5 Δf comparisons in Scenario I

4.3 Time domain simulation

The optimal parameters for VIC-FOPID and VIC-PID are tabulated in Table 5. These parameters are investigated by time domain simulation based on scenarios. The dynamic behavior of the system when minor disturbances occur is described, including the RoCoF or frequency nadir, overshoot, and settling time.

4.3.1. Scenario I

In Scenario I, the simulation investigates the effect of fluctuation and uncertainties of P_{WES} and P_{PVES} in the dynamic behavior of HRES. The investigation is focused on the Δf response as given in Fig. 5. Besides that, the Δf response is detailed in Table 6. The minor disturbances are simulated in specific times, there are 2, 7, and 12 s time simulations. Thus, it can be seen in the base case (Without VIC) that the oscillation occurs in 2 s, then the oscillation becomes higher in 7 s due to larger disturbances. In the situation without VIC, the worst frequency nadir occurred in HRES of -1.25 x 10^{-3} p.u. at 7.75 s. Besides that, the maximum overshoot occurred at 9.79 s of 1.21 x 10^{-3} p.u. After that, the residual disturbances in 12 s make the HRES return to its steady-state response after 18.54 s.

With VIC, the Δf response is significantly improved. The RoCoF is reduced which means frequency nadir also improved. Besides that, the maximum overshoot is damped properly resulting in a better settling time. The results show that the FOPID gives better stability improvement than the basic PID. The best improvement is achieved by VIC-FOPID-HHO with a frequency nadir of -1.32 x 10^{-4} p.u. at 7.09 s and a maximum overshoot of 1.87 x 10^{-5} p.u. at 10 s, which is 89.44% and 98.45% better than the base case without VIC, respectively. Moreover, the settling time is also significantly reduced by 61.48% of 7.14 s. These results justify the superiority of the proposed method in enhancing the stability of HRES with the fluctuation and uncertainties of P_{WES} and P_{PVES} dependent on the ΔP_{wind} and ΔP_{solar}, respectively.

Besides that, the improvement conducted by the other methods in Scenario I is given in the following:

VIC-FOPID-AOA, frequency nadir of -1.42 x 10^{-4} p.u. at 7.09 s, maximum overshoot of 2.07 x 10^{-5} p.u. at 10.7 s, and settling time 7.38 s, which are 88.64%, 98.28%, and 60.19% better than without VIC, respectively.

VIC-FOPID-EOA, frequency nadir of -2.67 x 10^{-4} p.u. at 7.19 s, maximum overshoot of 6.71 x 10^{-5} p.u. at 10.08 s, and settling time 7.84 s, which are 78.64%, 94.45%, and 57.71% better than without VIC, respectively.

Table 6. Detailed Δf response in Scenario I

Controller	Response		
	Frequency Nadir (p.u.)	Maximum Overshoot (p.u.)	Settling Time (s)
Without VIC	-1.25 x 10^{-3}	1.21 x 10^{-3}	18.54
VIC-FOPID-AOA	-1.42 x 10^{-4}	2.07 x 10^{-5}	7.38
VIC-FOPID-EOA	-2.67 x 10^{-4}	6.71 x 10^{-5}	7.84
VIC-FOPID-HHO	-1.32 x 10^{-4}	1.87 x 10^{-5}	7.14
VIC-PID-AOA	-2.11 x 10^{-4}	2.3 x 10^{-5}	7.36
VIC-PID-EOA	-1.52 x 10^{-4}	7.56 x 10^{-6}	7.11
VIC-PID-HHO	-1.69 x 10^{-4}	2.58 x 10^{-5}	7.48

VIC-PID-AOA, frequency nadir of -2.11 x 10^{-4} p.u. at 7.14 s, maximum overshoot of 2.3 x 10^{-5} p.u. at 9.1 s, and settling time 7.36 s, which are 83.12%, 98.09%, and 50.91% better than without VIC, respectively.

VIC-PID-EOA, frequency nadir of -1.52 x 10^{-4} p.u. at 7.07 s, maximum overshoot of 7.56 x 10^{-6} p.u. at 47.21 s, and settling time 7.11 s, which are 87.84%, 99.37%, and 61.65% better than without VIC, respectively. This result shows that improper parameters can lead to the surge of the oscillation over a very long time which is indicated by the maximum overshoot that occurred at 47.21 s. Even though, the overshoot value does not exceed the steady-state limit.

VIC-PID-HHO, frequency nadir of -1.69 x 10^{-4} p.u. at 7.2 s, maximum overshoot of 2.58 x 10^{-5} p.u. at 9.1 s, and settling time 7.48 s, which are 86.84%, 97.86%, and 59.65% better than without VIC, respectively.

4.3.2. Scenario II

In Scenario II, the simulation investigates the dynamic behavior of HRES when multi-level load shedding has occurred. The Δf response is given in Fig. 6. Besides that, the detailed response is given in Table 7. In 2 s, the load shedding occurs when the RES still supplying power to the load, it makes the overshoot very high as seen in the base case (Without VIC). The maximum overshoot reaches 5.69 x 10^{-4} p.u. at 3.18 s, while the frequency nadir of -2.3 x 10^{-}

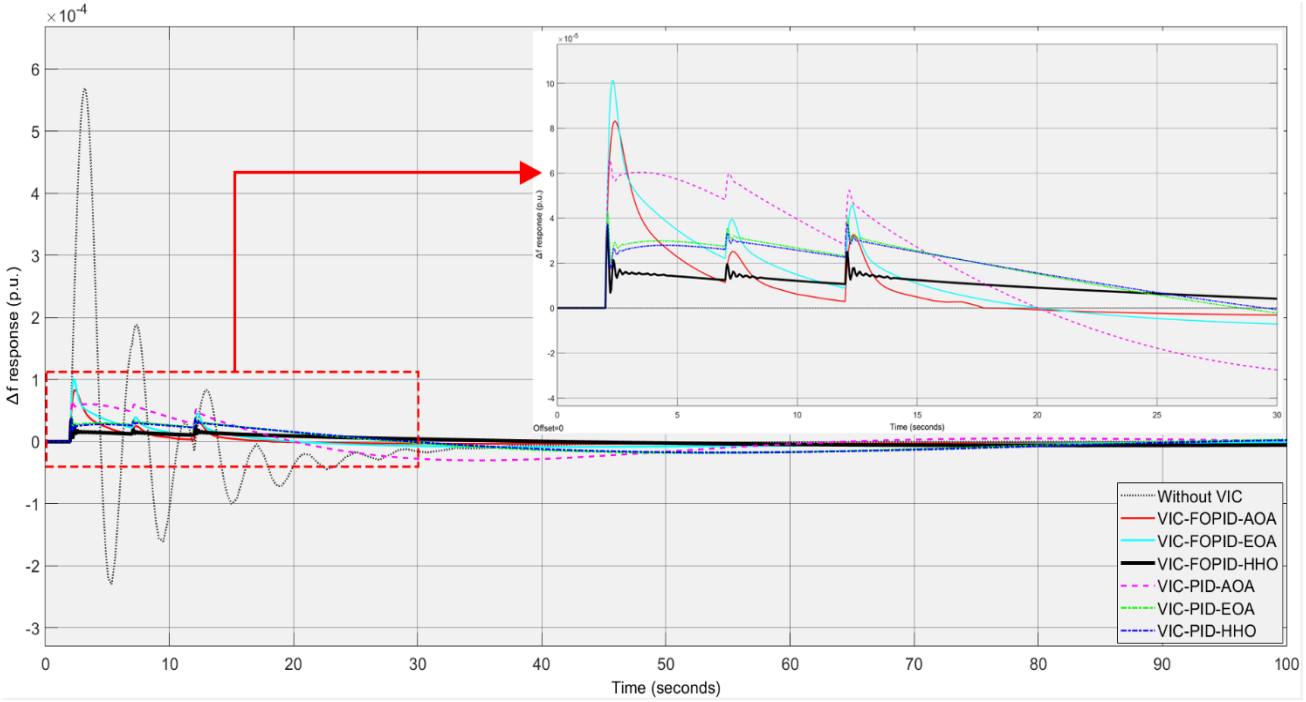

Figure. 6 Δf comparisons in Scenario II

Table 7. Detailed Δf response in Scenario II

Controller	Response		
	Frequency Nadir (p.u.)	Maximum Overshoot (p.u.)	Settling Time (s)
Without VIC	-2.3 x 10^{-4}	5.69 x 10^{-4}	36.18
VIC-FOPID-AOA	-5.97 x 10^{-6}	8.32 x 10^{-5}	13.57
VIC-FOPID-EOA	-8.58 x 10^{-6}	1.01 x 10^{-4}	15.32
VIC-FOPID-HHO	-5.89 x 10^{-6}	3.62 x 10^{-5}	18.11
VIC-PID-AOA	-3.02 x 10^{-5}	6.61 x 10^{-5}	54.5
VIC-PID-EOA	-1.81 x 10^{-5}	4.28 x 10^{-5}	73.18
VIC-PID-HHO	-1.74 x 10^{-5}	3.86 x 10^{-5}	75.32

^{4} p.u. at 5.345 s. the multi-level load shedding makes the settling time longer of 36.18 s.

The VIC addition is effective in dampening the oscillation when multi-level load shedding occurs. VIC-FOPID shows promising results, while the VIC-PID is a bit difficult in suppressing the frequency nadir reduction. The best improvement is achieved by VIC-FOPID-HHO. The VIC-FOPID-HHO can significantly dampen the overshoot by 93.67% of 3.62 x 10^{-5} p.u. at 2.1 s. The frequency nadir is also reduced by 97.4% of -5.89 x 10^{-6} p.u. However, the side effect from additional controllers like VIC makes the response take longer to return to its reference point. It can be seen from the frequency nadir occurred at 83.82 s. However, it is not a problem due to the VIC is proven to reduce the settling time of HRES to achieve the steady-state limit at 18.11 s. It is 49.94% better than the base case without VIC. These results prove the VIC-FOPID-HHO is superior in enhancing the stability of HRES when multi-level load shedding occurs.

Besides that, the improvement conducted by the other methods in Scenario II is given in the following:

VIC-FOPID-AOA, frequency nadir of -5.97 x 10^{-6} p.u. at 42.17 s, maximum overshoot of 8.32 x 10^{-5} p.u. at 2.4 s, and settling time 13.57 s, which are 98.44%, 85.37%, and 62.49% better than without VIC, respectively.

VIC-FOPID-EOA, frequency nadir of -8.58 x 10^{-6} p.u. at 39.6 s, maximum overshoot of 1.01 x 10^{-4} p.u. at 2.3 s, and settling time 15.32 s, which are 96.27%, 82.24%, and 57.65% better than without VIC, respectively.

VIC-PID-AOA, frequency nadir of -3.02 x 10^{-5} p.u. at 34.58 s and maximum overshoot of 6.61 x 10^{-5} p.u. at 2.2 s, which are 86.87% and 88.38% better than without VIC, respectively. However, the settling time of VIC-PID-AOA is 54.5 s, which is 50.63% longer than without VIC.

VIC-PID-EOA, frequency nadir of -1.81 x 10^{-5} p.u. at 51.82 s and maximum overshoot of 4.28 x 10^{-5} p.u. at 2.1 s, which are 92.13% and 92.47% better than without VIC, respectively. However, the settling time of VIC-PID-EOA is 73.8 s, which is 102.26% longer than without VIC.

VIC-PID-HHO, frequency nadir of -1.74 x 10^{-5} p.u. at 55.83 s and maximum overshoot of 3.86 x 10^{-5} p.u. at 2.1, which are 92.43% and 93.21% better than without VIC, respectively. However, the settling time of VIC-PID-HHO is 75.32 s, which is 108.18% longer than without VIC.

5. Conclusion

The stability improvement of HRES is proposed by using VIC-FOPID-HHO. HRES is designed with in simple model to focus the investigation on the dynamic behavior of the system. HRES consists of SGES, WES, PVES, and ESU to realize the VI emulation. The proposed method is evaluated with two scenarios representing the RES behavior condition, and multi-level sudden power load shedding. The main findings supporting the significant contribution of this paper are summarized in the following:

1) The superiority of HHO over AOA and EOA in optimizing VIC-FOPID and VIC-PID is observable in statistical assessment and convergence curves. The optimal solution provided by HHO is 41.62% and 31.98% better than AOA and EOA, respectively.
2) Scenario I simulates the fluctuation and uncertainties of RES in supplying power load demand. In this scenario, P_{WES} and P_{PVES} are dependent on the ΔP_{wind} and ΔP_{solar}, respectively. The VIC-FOPID-HHO is proven to conduct the best stability improvement with frequency nadir improvement of 89.44% and maximum overshoot reduction of 98.45%. Moreover, the settling time is 61.48% better than the base case.
3) Scenario II simulates the HRES when multi-level load shedding occurs. The very high overshoot can be dampened significantly with VIC-FOPID-HHO of 93.67% compared to the base case. Besides that, the frequency nadir also improved by 97.4%. Moreover, the settling time is 49.94% better than the base case.

Considering the success of VIC-FOPID-HHO in improving the stability of HRES, further investigation should be conducted in future work. The investigation can be implemented in more complex systems like interconnected power systems with multi-machines and multi-areas. Besides that, the ESU model for VI emulation can be detailed with different types of recent novel ESU models.

Nomenclature

Avg.	Average in statistic
B_L	Lower bound
B_U	Upper bound
E_{esc}	Escaping energy of the rabbit
E_o	Initial energy of the rabbit
D	Damping properties
D_{VI}	Virtual damping
H	Inertia properties
H_i	Initial position of the hawk in HHO
H_m	Average of the position of the hawk
H_{rand}	Random hawk
$H(T)$	Position of the hawk
J	Jumping movement of HHO
K_D	Derivative gain
K_I	Integral gain
K_P	Proportional gain
K_s	Contant in the secondary *f* controller
LF	Levy flight
N_{pop}	Number of population in HHO
P_{gov}	Generated power in the turbine
P_{load}	Power load demand
P_m	Change of mechanical power in SGES
P_{solar}	Solar irradiation level
P_{VI}	Virtual inertia
P_{wind}	Wind speed level
q	Parameter for movement of the hawk
R	Speed droop controller
r_{esc}	Probability of the rabbit escaping
R_i	Rabbit position
R_{VI}	Virtual inertia droop
r_1, r_2, r_3, r_4, r_5,	Randomly uniform distribution values between 0 to 1 in HHO
Std.dev.	Standard deviation in statistic
T	Iteration
T_{ESU}	Time response of ESU
T_{gov}	Time response of the governor in SGES
T_{INV}	Time response of inverter
T_{PVES}	Time response of PVES
T_{max}	Maximum iteration
T_{tur}	Time response of the turbine in SGES
T_{sim_max}	Maximum of the time simulation
T_{WES}	Time response of WES
V_{FOPID}	FOPID output
Δf	RoCoF
ΔV_{ref1}	Reference signal from the primary *f* controller
ΔV_{ref2}	Reference signal from the secondary *f* controller
ΔV_{ref3}	Reference signal for ESU to generate VI emulation
β	Bias factor
σ_{eig}	Damping factor
ξ_{eig}	Damping ratio
λ, μ	Fractional order
λ_{eig}	Eigenvalue of the system
ω_{eig}	Oscillation factor

List of Abbreviation

AOA	Arithmetic Optimization Algorithm
EOA	Equilibrium Optimization Algorithm

ESU	Energy Storage Unit
FLC	Fuzzy Logic Controller
FA	Firefly Algorithm
FOPID	Fractional Order Proportional-Integral-Derivative
FPA	Flower Pollination Algorithm
HHO	Harris Hawk Optimization
HRES	Hybrid Renewable Energy Systems
ITAE	Integral Time Absolute Error
MRFA	Manta Ray Foraging Algorithm
PSS	Power System Stabilizer
PVES	Photovoltaic Energy Systems
RoCoF	Rate of Change of Frequency
SGES	Synchronous Generator Energy Systems
SVC	Static VAR Compensator
VIC	Virtual Inertia Controller
WES	Wind Energy Systems

Conflicts of Interest

The authors declare no conflicts of interest.

Author Contributions

Conceptualization, IR and MAP; methodology, IR, MAP, and MRD; software, MAP, MRD, and AR; validation, VLBP and RSW; formal analysis, MAP; investigation, IR; resources, MRD; data curation, AR; writing—original draft preparation, MAP; writing—review and editing, IR; visualization, MAP; supervision, IR; project administration, VLBP and RSW; funding acquisition, IR.

Acknowledgments

This work is supported by the Directorate of Research and Community Service (Direktorat Riset, Teknologi, dan Pengabdian kepada Masyarakat, DRPM), Ministry of Education, Culture, Research, and Technology (Kementerian Pendidikan, Kebudayaan, Riset dan Teknologi, Kemendikbudristek) of the Republic of Indonesia under grant number 1760/PKS/ITS/2024.

References

[1] Subiyanto, M. A. Prakasa, P. Wicaksono, and M. A. Hapsari, "Intelligence technique based design and assessment of photovoltaic-battery-diesel for distributed generation system in campus area", *Int. Rev. Model. Simulations*, Vol. 13, No. 1, 2020, doi: 10.15866/iremos.v13i1.18147.

[2] Q. Hassan *et al.*, "A comprehensive review of international renewable energy growth", *Energy Built Environ.*, No. 2023, 2024, doi: 10.1016/j.enbenv.2023.12.002.

[3] J. C. León Gómez, S. E. De León Aldaco, and J. Aguayo Alquicira, "A Review of Hybrid Renewable Energy Systems: Architectures, Battery Systems, and Optimization Techniques", *Eng*, Vol. 4, No. 2, pp. 1446–1467, 2023, doi: 10.3390/eng4020084.

[4] M. R. Djalal, I. Robandi, and M. A. Prakasa, "Stability Enhancement of Sulselrabar Electricity System Using Mayfly Algorithm Based on Static Var Compensator and Multi-Band Power System Stabilizer PSS2B", *IEEE Access*, Vol. 11, pp. 57319–57340, 2023, doi: 10.1109/ACCESS.2023.3283598.

[5] N. Nikolaev, K. Dimitrov, and Y. Rangelov, "A comprehensive review of small-signal stability and power oscillation damping through photovoltaic inverters", *Energies*, Vol. 14, No. 21, 2021, doi: 10.3390/en14217372.

[6] T. Kerdphol, F. S. Rahman, M. Watanabe, and Y. Mitani, *Virtual Inertia Synthesis and Control*. 2021. [Online]. Available: https://link.springer.com/book/10.1007/978-3-030-57961-6%0Ahttp://link.springer.com/10.1007/978-3-030-57961-6

[7] M. A. Prakasa, I. Robandi, R. Nishimura, and M. R. Djalal, "A New Scheme of Harris Hawk Optimizer with Memory Saving Strategy (HHO-MSS) for Controlling Parameters of Power System Stabilizer and Virtual Inertia in Renewable Microgrid Power System", *IEEE Access*, Vol. 12, pp. 73849–73878, 2024, doi: 10.1109/ACCESS.2024.3385089.

[8] M. A. Prakasa, I. Robandi, R. Nishimura, and M. R. Djalal, "A Hybrid Controlling Parameters of Power System Stabilizer and Virtual Inertia Using Harris Hawk Optimizer in Interconnected Renewable Power Systems", *IEEE Access*, Vol. 12, 2024, doi: 10.1109/ACCESS.2024.3405994.

[9] D. Alonso Sørensen, D. Vázquez Pombo, and E. Torres Iglesias, "Energy storage sizing for virtual inertia contribution based on ROCOF and local frequency dynamics", *Energy Strateg. Rev.*, Vol. 47 , 2023, doi: 10.1016/j.esr.2023.101094.

[10] B. N. Syifa, D. A. Asfani, A. Priyadi, and H. Setiadi, "Frequency Stability Analysis on Optimization of Virtual Inertia Controller Settings Based on Retired Electric Vehicles Battery Using Firefly Algorithm", In: *Proc. of Int. Conf. Comput. Eng. Netw. Intell. Multimedia, CENIM 2022*, pp. 365–370, 2022, doi: 10.1109/CENIM56801.2022.10037414.

[11] A. N. A. Maulidhia, D. A. Asfani, A. Priyadi,

and H. Setiadi, "Frequency Stability Analysis on Optimization of Virtual Inertia Control (VIC) Capacitor Energy Storage (CES) Controller Settings Using Particle Swarm Optimization", In: *Proc. of Int. Conf. Comput. Eng. Netw. Intell. Multimedia, CENIM 2022*, No. Vic, pp. 359–364, 2022, doi: 10.1109/CENIM56801.2022.10037313.

[12] A. Saleh, W. A. Omran, H. M. Hasanien, M. Tostado-Véliz, A. Alkuhayli, and F. Jurado, "Manta Ray Foraging Optimization for the Virtual Inertia Control of Islanded Microgrids Including Renewable Energy Sources", *Sustain.*, Vol. 14, No. 7, 2022, doi: 10.3390/su14074189.

[13] A. Mohamed, H. Elzoghby, M. Bahgat, and A. G. Mohamed, "Enhanced Non-linear PID-Based on Virtual Inertia Control to Enhance the Frequency Stability of a Hybrid Power System", *Int. J. Adv. Eng. Bus. Sci.*, Vol. 0, No. 0, pp. 1–18, 2022, doi: 10.21608/ijaebs.2022.155614.1029.

[14] M. A. E. Mohamed, K. Jagatheesan, and B. Anand, "Modern PID/FOPID controllers for frequency regulation of interconnected power system by considering different cost functions", *Sci. Rep.*, Vol. 13, No. 1, pp. 1–29, 2023, doi: 10.1038/s41598-023-41024-5.

[15] G. Sahoo, R. K. Sahu, S. Panda, N. R. Samal, and Y. Arya, "Modified Harris Hawks Optimization-Based Fractional-Order Fuzzy PID Controller for Frequency Regulation of Multi-Micro-Grid", *Arab. J. Sci. Eng.*, Vol. 48, No. 11, pp. 14381–14405, 2023, doi: 10.1007/s13369-023-07613-2.

[16] V. Skiparev, J. Belikov, E. Petlenkov, and Y. Levron, "Reinforcement Learning based MIMO Controller for Virtual Inertia Control in Isolated Microgrids", *IEEE PES Innov. Smart Grid Technol. Conf. Eur.*, Vol. 2022-Octob, pp. 1–5, 2022, doi: 10.1109/ISGT-Europe54678.2022.9960447.

[17] S. B. Joseph, E. G. Dada, A. Abidemi, D. O. Oyewola, and B. M. Khammas, "Metaheuristic algorithms for PID controller parameters tuning: review, approaches and open problems", *Heliyon*, Vol. 8, No. 5, p. e09399, 2022, doi: 10.1016/j.heliyon.2022.e09399.

[18] K. Hongesombut and R. Keteruksa, "Fractional order based on a flower pollination algorithm PID controller and virtual inertia control for microgrid frequency stabilization", *Electr. Power Syst. Res.*, Vol. 220, p. 109381, 2023, doi: 10.1016/j.epsr.2023.109381.

[19] F. Amiri, M. Eskandari, and M. H. Moradi, "Virtual Inertia Control in Autonomous Microgrids via a Cascaded Controller for Battery Energy Storage Optimized by Firefly Algorithm and a Comparison Study with GA, PSO, ABC, and GWO", *Energies*, Vol. 16, No. 18, 2023, doi: https://doi.org/10.3390/en16186611.

[20] C. Rohmingtluanga *et al.*, "Enhanced harris hawks optimization based load frequency control of multi area microgrid based water treatment plant with consideration of 3DOF-(FO-PIDN)/(TIDN) controller", *Front. Energy Res.*, Vol. 12, No. April, pp. 1–24, 2024, doi: 10.3389/fenrg.2024.1387780.

[21] D. Yousri, T. S. Babu, and A. Fathy, "Recent methodology based Harris Hawks optimizer for designing load frequency control incorporated in multi-interconnected renewable energy plants", *Sustain. Energy, Grids Networks*, Vol. 22, p. 100352, 2020, doi: 10.1016/j.segan.2020.100352.

[22] A. Asghar, S. Mirjalili, H. Faris, and I. Aljarah, "Harris hawks optimization : Algorithm and applications", *Futur. Gener. Comput. Syst.*, Vol. 97, pp. 849–872, 2019, doi: 10.1016/j.future.2019.02.028.

[23] M. Shehab *et al.*, "Harris Hawks Optimization Algorithm: Variants and Applications", *Arch. Comput. Methods Eng.*, Vol. 29, No. 7, pp. 5579–5603, 2022, doi: 10.1007/s11831-022-09780-1.

[24] B. K. Tripathy *et al.*, "Harris Hawk Optimization: A Survey onVariants and Applications", *Comput. Intell. Neurosci.*, Vol. 2022, 2022, doi: 10.1155/2022/2218594.

[25] A. Faramarzi, M. Heidarinejad, B. Stephens, and S. Mirjalili, "Equilibrium optimizer: A novel optimization algorithm", *Knowledge-Based Syst.*, Vol. 191, p. 105190, 2020, doi: 10.1016/j.knosys.2019.105190.

[26] L. Abualigah, A. Diabat, S. Mirjalili, M. Abd Elaziz, and A. H. Gandomi, "The Arithmetic Optimization Algorithm", *Comput. Methods Appl. Mech. Eng.*, Vol. 376, p. 113609, 2021, doi: 10.1016/j.cma.2020.113609.

[27] M. A. Prakasa and I. Robandi, "Tuning Improvement of Power System Stabilizer using Hybrid Harris Hawk Optimization-Equilibrium Optimizer Algorithm", In: *Proc. of 2022 6th Int. Conf. Inf. Technol. Inf. Syst. Electr. Eng. 2022*, pp. 553–558, 2022.

[28] M. Nour *et al.*, "A New Fractional-Order Virtual Inertia Support Based on Battery Energy Storage for Enhancing Microgrid Frequency Stability", *Fractal Fract.*, Vol. 7,

No. 12, pp. 1–22, 2023, doi: 10.3390/fractalfract7120855.

[29] W. Zheng, Y. Luo, Y. Chen, and X. Wang, "A simplified fractional order pid controller's optimal tuning: A case study on a pmsm speed servo", *Entropy*, Vol. 23, No. 2, pp. 1–21, 2021, doi: 10.3390/e23020130.

[30] M. Izdebski, R. Małkowski, and P. Miller, "New Performance Indices for Power System Stabilizers", *Energies*, Vol. 15, No. 24, 2022, doi: 10.3390/en15249582.

[31] A. Y. Jaen-Cuellar, R. D. J. Romero-Troncoso, L. Morales-Velazquez, and R. A. Osornio-Rios, "PID-controller tuning optimization with genetic algorithms in servo systems", *Int. J. Adv. Robot. Syst.*, Vol. 10, 2013, doi: 10.5772/56697.